crystals

MDPI

Article

The Mechanism of High-Strength Quenching-Partitioning-Tempering Martensitic Steel at Elevated Temperatures

Ke Zhang [1,*], Maoyuan Zhu [1], Bitong Lan [1], Ping Liu [1], Wei Li [1] and Yonghua Rong [2]

[1] School of Materials Science and Engineering, University of Shanghai for Science and Technology, Shanghai 200093, China; 15901866360@163.com (M.Z.); lanbitongjxy@163.com (B.L.); liuping@usst.edu.cn (P.L.); liwei176@usst.edu.cn (W.L.)

[2] School of Materials Science and Engineering, Shanghai Jiao Tong University, Shanghai 200240, China; yhrong@sjtu.edu.cn

* Correspondence: zhangke@usst.edu.cn; Tel.: +86-21-5527-0943

Received: 11 December 2018; Accepted: 1 February 2019; Published: 13 February 2019

Abstract: High-strength medium-carbon martensitic steel was heat treated through a quenching-partitioning-tempering (Q-P-T) treatment. Both the mechanism for improved ductility and the high temperature stability of austenite were investigated. The Q-P-T martensitic steel showed good products of strength and elongation (PSE) at various deformation temperatures ranging within 25–350 °C. The optimum PSE value (>57,738 MPa%) was achieved at 200 °C. The microstructure of the Q-P-T steel is constituted of laths martensite with dislocations, retained austenite located within lath martensite and small niobium carbides (NbC), and/or transitional ε-carbides that precipitated in the lath martensite. The good ductility can be mainly attributed to the laminar-like austenite that remained within the lath-martensite. The austenite can effectively enhance ductility through the effect of dislocation absorption by the retained austenite and through transformation-induced plasticity. The relationship between the microstructures and mechanical properties was investigated at high deformation temperatures.

Keywords: quenching-partitioning-tempering steel; retained austenite; mechanical stability; microstructure

1. Introduction

The quenching and partitioning (Q&P) process [1,2] has been put forward and applied in advanced high-strength steels (AHSSs) to achieve excellent ductility and strength. The core concept is based on the carbon distribution process from supersaturated martensite to untransformed austenite. The process is conducted to provide sufficient time at either the initial quenching temperature or above, and to thus stabilize the retained austenite to an ambient temperature. At present, the Q&P process has gradually evolved to quenching-partitioning-tempering (Q-P-T) [3], direct quenching and partitioning (DQ&P) [4,5], and quenching and tempering-associated partitioning (Q-T&P) [6]. The Q-P-T treatment emphasized the application of precipitation strengthening to the Q&P process. The main differences between the Q&P and Q-P-T processes are as follows: (i) The microalloying elements (Nb and V) are included in the Q-P-T process, which can result in grain refinement and carbides precipitation, but they are not included in the Q&P process. (ii) The tempering time and temperature depend on the proper carbides precipitation rather than the carbon partitioning process, and tempering includes partitioning. Thus, the metallography of such steels consists of lath martensite, laminar-like retained austenite located within lath-martensite, and fine carbides dispersed throughout the martensite matrix.

Our previous research has clarified that Q-P-T steels possess a superior combination of ductility and strength at an ambient temperature [7–10].

The effects of microalloying elements, quenching and partitioning temperatures, holding time, and martensite/austenite interface migration on the mechanical properties and microstructure of steels have been extensively investigated [11–15]. In particular it has been shown that silicon, aluminum, and manganese can be utilized for the stabilization of retained austenite at ambient temperatures [16–18]. However, few studies have elucidated the relationship between mechanical properties and deformed temperatures [19,20]. Q-P-T steels have been applied in automobiles as a kind of AHSSs. The service conditions of engineering components such as a high temperature and strain rate are becoming increasingly complex. In the study of mechanical properties, temperature is one of the influencing factors. Accordingly, this work aimed to demonstrate the influence of deformation temperature on the mechanical properties and the microstructure of the Q-P-T steel, to reveal the degree of austenite stability at high temperatures, and to determine a temperature range favorable for the processing of Q-P-T martensitic steel.

2. Experimental Procedure

Table 1 lists the chemical compositions of the Q-P-T martensitic steel used in this study. Si is chosen to inhibit the formation of cementite [1]. Manganese is added to stabilize the untransformed austenite and to reduce the M_s temperature. Niobium is selected to form the stable carbides precipitation and refine the parent austenite grain to enhance strength [21]. The A_{c3}, M_s, and M_f temperatures, also listed in Table 1, were calculated from the dilatometric data obtained with a Formaster FII dilatometer (Fuji Industry Inc., Tokyo, Japan).

Table 1. Chemical compositions (wt%) and the temperature of A_{c3} and M_s.

C	Mn	Si	Nb	S	P	A_{c3} (°C)	M_s (°C)	M_f (°C)
0.42	1.46	1.58	0.028	<0.01	<0.01	797 ± 5	289 ± 5	84 ± 3

The 12-mm-thick hot-rolled plate was supplied by the Central Iron and Steel Research Institute, Beijing, China. The 2-mm-thick samples were tailored from the hot-rolled plate for Q-P-T treatment. First, the sample was austenitized at 850 °C for 300 s, followed by rapid quenching (about 15 s) to 200 °C in a salt bath; the sample was then transferred to molten salt at 450 °C and held there for 30 s. Finally, the sample was quenched with water to an ambient temperature. The optimal quenching temperature was predicted based on the combination of the kinetics K-M equation [22] and the constrained carbon equilibrium (CCE) model [1]. To prevent tempering brittleness, the selected tempering temperature was set at 450 °C [7,8].

The tensile tests at different high temperatures (25–350 °C) were conducted on a SANS 5105 machine (MTS Systems Corporation, Shanghai, China) at a strain rate of 0.5 mm/min. The tensile samples were cut into rectangular shapes with a 5 mm width and 15 mm length. Before the tests, all samples were kept at each high temperature for approximately 600 s to ensure that the temperatures of the samples were fully uniform. Moreover, two samples were used to obtain the average value of the mechanical properties for each high-temperature tensile test. The microstructures of the deformed and undeformed samples were observed through a transmission electron microscope (TEM). The deformed and undeformed TEM specimens were selected from the vicinity of the fracture and the root of the tensile sample, respectively. The specimens for the TEM observation were first prepared via mechanical grinding before slices were punched. Following this, the slices were electropolished by using a twin-jet polisher with 4% perchloric acid in ethanol as a corrosive agent at −20 °C. The TEM tests was conducted in a JEOL-2100F microscope (JEOL Company, Tokyo, Japan). The phases of the undeformed samples were characterized by using a D/max-2550 X-ray diffractometer (XRD, Rigaku Corporation, Tokyo, Japan) at a scanning speed of 5°/min, ranging from 35°–105°. After being held

for 600 s, the volume fraction of retained austenite (V_{RA}) was obtained by a direct comparison method with the integrated intensity of the austenite peaks of $(200)_\gamma$, $(220)_\gamma$, and $(311)_\gamma$ and the martensite peaks of $(200)_\alpha$ and$(211)_\alpha$.

3. Results and Discussion

The variation of the ultimate tensile strength (UTS), the total elongation (A) and the products of strength and elongation (PSE) of these steels with an increased tensile temperature is displayed in Figures 1a and 1b, respectively. The mechanical properties present the following three-stages variation: (1) When the temperature range I was between 25 °C and 150 °C, A, UTS and PSE remained almost unchanged, which indicates that this Q-P-T steel was at its most stable temperature stage; (2) When the temperature range II was between 150 °C and 200 °C, the variation of A, UTS and PSE exhibited the same trend, and they all increased rapidly. In particularthe samples had an A of 35.2%, a UTS of 1640 MPa, and a PSE of 57,738 MPa% when the tensile samples were deformed at 200 °C; and (3) When the temperature range III was higher than 200 °C, the A, UTS and PSE values of the deformed samples gradually weakened with an increased tensile temperature. However, the composite mechanical properties of the samples after deformation at 350 °C were as good as those at atmosphere temperature. Therefore, this Q-P-T martensitic steel exhibited superior mechanical properties combined with elongation and strength within the temperature range of 25–350 °C. These results were consistent with those obtained in our previous studies [15,19], wherein low-carbon martensitic steels (0.2 wt% C) subjected to Q-P-T treatment possessed a temperature regime with good mechanical properties.

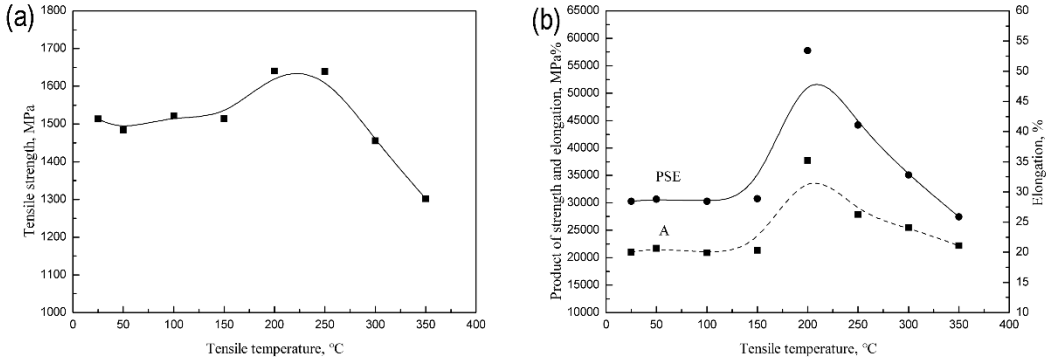

Figure 1. Tensile properties of the quenching-partitioning-tempering (Q-P-T) martensitic steels with an increased test temperature: (**a**) the ultimate tensile strength (UTS) (**b**) the total elongation (A), and the products of strength and elongation (PSE).

Figure 2a shows the XRD pattern of the sample without deformation held for 600 s in the deformation temperature range of 25–350 °C. The XRD spectra show that the treated samples consist of both retained austenite and martensite. Meanwhile, the intensity of the spectra of the retained austenite decreased gradually with increased deformation temperatures. V_{RA} in non-deformed specimens can be used as a criterion for determining the thermal stability of medium carbon Q-P-T martensitic steel at various high deformation temperatures, which can be obtained by XRD analysis. The V_{RA} values were determined, as shown in Figure 2b; they decreased slowly at 25–200 °C and then decreased quickly at temperatures above 200 °C. The V_{RA} remained nearly unchanged at 16%, thereby corresponding to the first stage of the mechanical properties with increased temperatures, showing that the retained austenite exhibits good thermal stability. In the second stage, the V_{RA} decreased slightly from 16% to 14.9%. This finding may be attributed to the fact that high temperatures reduced the driving force of the martensitic transformation. Thus, a larger strain is required to induce the martensitic transition, thereby expanding the strain range of the transformation-induced plasticity (TRIP) effect. However,

in the third stage, the V_{RA} quickly decreased to 7.93%, which can be ascribed to the decomposition of the retained austenite due to higher temperatures.

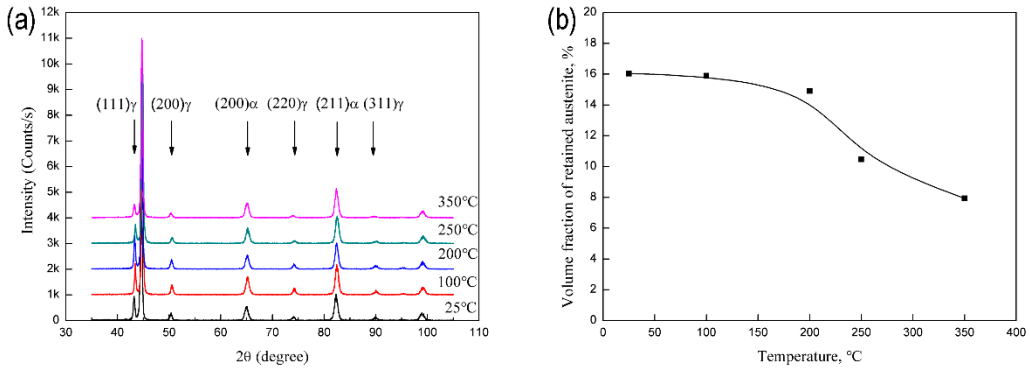

Figure 2. The steel held at different temperatures for 600 s: (**a**) XRD spectra; (**b**) evolution of V_{RA} versus deformed temperature.

The effects of the microstructural changes on the mechanical properties of the three typical specimens deformed at 25 °C, 200 °C and 350 °C were characterized by TEM. For a comparison, the undeformed specimens were also characterized. The bright field (BF) and the dark field (BF) images of the Q-P-T specimen without deformation at an ambient temperature are shown in Figures 3a and 3b, respectively. The investigated Q-P-T specimens presented the typical micro-structure: dislocation-type lath martensite and laminar-like retained austenite distributed within lath martensite. The result of the selected area electron diffraction (SAED) patterns confirmed the orientation relationships (ORs) between lath martensite and the laminar-like retained austenite as the Kurdjumov-Saches (K-S) relationship $[\bar{1}\bar{1}1]_\alpha // [0\bar{1}\bar{1}]_\gamma$, $(1\bar{1}0)_\alpha // (11\bar{1})_\gamma$, and the Nishiyama-Wassermann (N-W) relationship $[00\bar{1}]_\alpha // [0\bar{1}\bar{1}]_\gamma$, $(\bar{1}10)_\alpha // (11\bar{1})_\gamma$. Figure 4 shows the TEM images of the carbides in this Q-P-T martensitic steel without deformation at an ambient temperature. Two different carbides were clearly shown, including a granular and a flaky carbide. The BF image in Figure 4a and DF image in Figure 4b show many granular carbides with an average size of approximately 10 nm and a small amount of fine flaky carbides, all of which were dispersedly precipitated throughout the martensite matrix. The carbides with a granular form are fcc-niobium carbides (NbC), and those with a laminar form are transition type ε carbides, as identified by the SAED inserted in Figure 4b (indicated by the arrow in the figure). The addition of Si can only inhibit cementite precipitation but cannot inhibit transition type hcp-ε carbide precipitation.

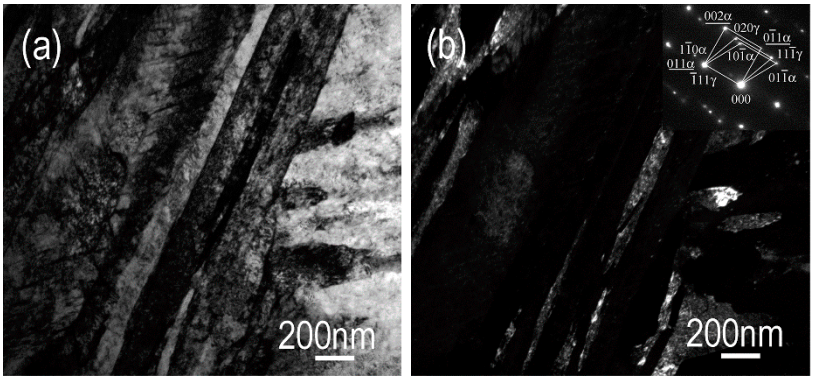

Figure 3. (**a**) Bright field (BF) and (**b**) Dark field (DF) micrographs of the retained austenite at 25 °C, with the corresponding selected area electron diffraction (SAED) pattern shown in (**b**).

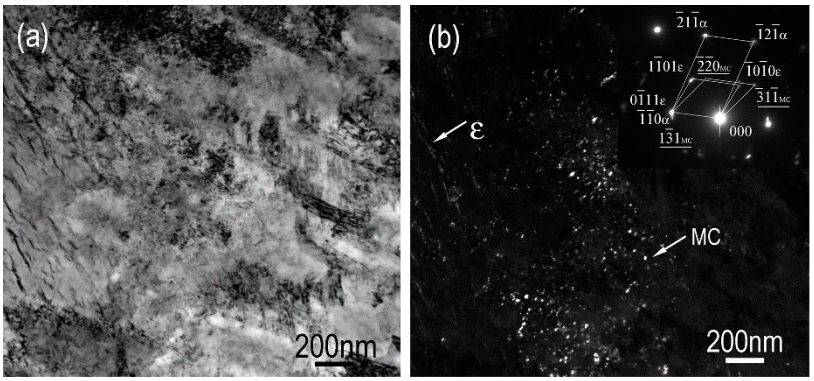

Figure 4. (**a**) BF and (**b**) DF micrographs of carbides at 25 °C, with the corresponding SAED pattern shown in (**b**).

The BF and DF images of the Q-P-T specimen without deformation at 200 °C are shown in Figures 5a and 5b, respectively. Similarly, the microstructure of the present specimen consists of lath martensite and laminar-like retained austenite within lath martensite. The result of the SAED confirmed the OR between lath martensite and the laminar-like retained austenite as being a K-S relationship: $[1\bar{1}\bar{1}]_{\alpha}//[0\bar{1}\bar{1}]_{\gamma}$, $(110)_{\alpha}//(11\bar{1})_{\gamma}$. The dark field image shows that the retained austenite in the non-deformed Q-P-T steel held for 600 s at 200 °C has a larger proportion, which was confirmed thanks to the analysis of previous XRD results.

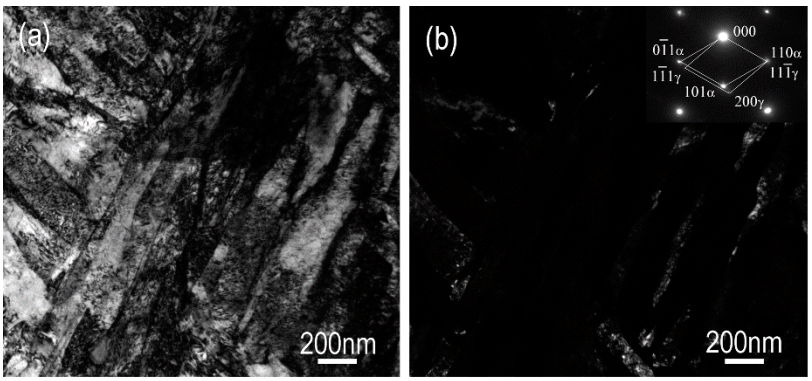

Figure 5. (**a**) BF and (**b**) DF micrographs of the retained austenite at 200 °C, with the corresponding SAED pattern inserted in (**b**).

The BF and DF images of the precipitated phases in the undeformed specimen at 200 °C are shown in Figures 6a and 6b, respectively. The flaky carbides were identified as transition type ε carbides based on the SAED patterns. The tempering temperature at 200 °C promoted a large amount of precipitation of the transition type ε carbides throughout the martensite matrix, and this was due to the high carbon content in the Q-P-T martensitic steel. During carbon partitioning, the precipitation of transition carbides reduced the amount of carbon atoms in the lath martensite, causing the martensite to soften and reducing the strength of the martensite matrix. However, with an increased tempering temperature, many carbides precipitated in the martensite, resulting in a pronounced precipitation strengthening effect [7–10]. This phenomenon is confirmed by Figure 1. In the first stage of the deformation, the UTS of this Q-P-T sample remained nearly constant before increasing rapidly to 1640 MPa at 200 °C for 600 s. The precipitation strengthening effect of the carbides exceeded the softening effect of the martensite matrix, thereby resulting in an obvious increase in the strength of the sample. Meanwhile, the Q-P-T sample exhibited the highest PSE at 200 °C. Sugimoto et al. [23] concluded that when the stability of the retained austenite is relatively high at a certain temperature range, the deformation resistance can within a certain stress range be increased by strain-strengthening via dislocation accumulation; it can

also be increased by reducing the axial stress, which transfers directly to the retained austenite. This therefore inhibits the occurrence of martensite transformation in the early strain stage and improves the elongation, especially the uniform elongation. We have recently proposed the dislocation absorption by retained austenite (DARA) effect [8–10]. With an increased strain from 0% to 3% and then to 19%, the average dislocation density of martensite initially decreased and then slowly increased from 6.65×10^{14} m^{-2} to 5.25×10^{14} m^{-2} and then to 7.48×10^{14} m^{-2}. Accordingly, the average dislocation density of austenite increased rapidly from 5.56×10^{14} m^{-2} to 42.98×10^{14} m^{-2}. The DARA effect induced the softening of martensite at the stage of uniform deformation, so the deformability of martensite matrix was markedly enhanced. The higher strength of this Q-P-T steel was therefore derived from the abundance of fine carbides (NbC and ε) dispersed throughout the martensite matrix, and a high plasticity resulted from the abundance of the retained austenite.

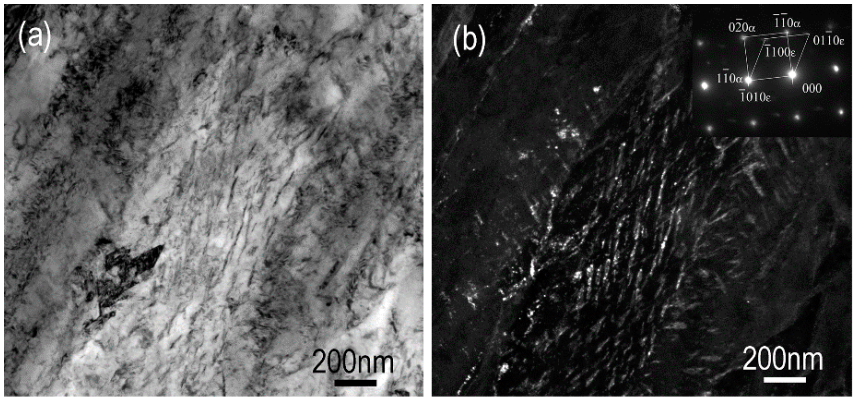

Figure 6. (**a**) BF and (**b**) DF micrographs of transition carbides at 200 °C, the corresponding SAED pattern inserted in (**b**).

The BF and DF images of the Q-P-T specimen without deformation held at 350 °C for 600 s are shown in Figures 7a and 7b, respectively. The V_{RA} decreased with a rise in temperature, and the laminar shape was not obvious and had a clear decomposition. The XRD results in Figure 2 show a consistent phenomenon. The retained austenite decomposed and transformed into ferrite and carbide with a rise in the tempering temperature. Figure 8 shows the TEM images of the MC carbides in the undeformed Q-P-T specimen at 350 °C. Figures 8a and 8c show the BF images of carbides. The carbides were identified as NbC and Fe_3C according to the SAED patterns shown in Figures 8b and 8d, respectively. With an increased tempering temperature, the fine NbC carbides dispersed throughout the martensite matrix coarsened gradually. At the same time, some of the transitional ε carbides were transformed into cementite, and the partially retained austenite decomposed into ferrite and cementite. The mechanical properties indicated that with a continuously increased temperature from 200 °C, the UTS, A, and PSE began to decrease. This finding was mainly derived from the transformation of transitional ε carbides into cementite and the decomposition of some retained austenite into ferrite + cementite, thereby resulting in a decrease of the V_{RA} and an increase of brittle cementite. In the Q-P-T martensitic steel, Si inhibited the formation of cementite in the low-temperature stage (25–200 °C) but not in the high-temperature stage (350 °C).

Figures 9a, 9b and 9c show the microstructures of these samples adjacent to the tensile fracture of the deformed Q-P-T steels at 25 °C, 200 °C, and 350 °C, respectively. The main characters of the deformed specimens are considerably entangled dislocations and partial subgrains formed in the lath martensite. Moreover, in this work, the plastic deformation formed many twin martensite plates via the carbon-rich retained austenite. As shown in Figure 10, twin martensite plates were observed in the TEM images of the specimens deformed at 25 °C, 200 °C, and 350 °C, respectively. Many twin martensite plates were parallel-distributed in the Q-P-T steel, as shown in BF images of Figures 10a, 10c and 10e, DF images of Figures 10b, 10d and 10f, respectively. The interfaces of the lath martensite and

the austenite are clearly shown in Figure 10d, which also revealed the parallel twin-type martensite plates distributed in the laminar-retained austenite. The SAED patterns of the twin-type martensite inserted in Figure 10b, Figure 10d, and Figure 10f showed that the lattice deviated from the original position, thereby indicating that the twin-type martensites underwent a high degree of deformation and distortion. DARA and TRIP effects can relax the stress concentration in a local area and redistribute stress during the plastic deformation. Meanwhile, many parallel twins increased the resistance of the high-strain region and the adjacent strain zone to continuous deformation, while also promoting the deformation of other regions with a lower strain and less twin interface by slipping until the formation of twins. Consequently, the deformation was uniform and the start of necking to the high-strain region was delayed [24]. The average elongation of the Q-P-T martensitic steel was 35.2% at 200 °C, thereby indicating that at this temperature, the formation of cracks was efficiently inhibited by DARA and TRIP effects.

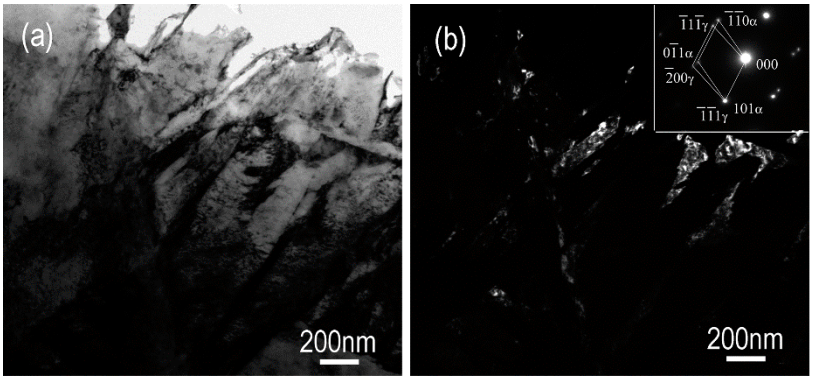

Figure 7. (**a**) BF and (**b**) DF micrographs of the retained austenite at 350 °C, with the corresponding SAED pattern inserted in (**b**).

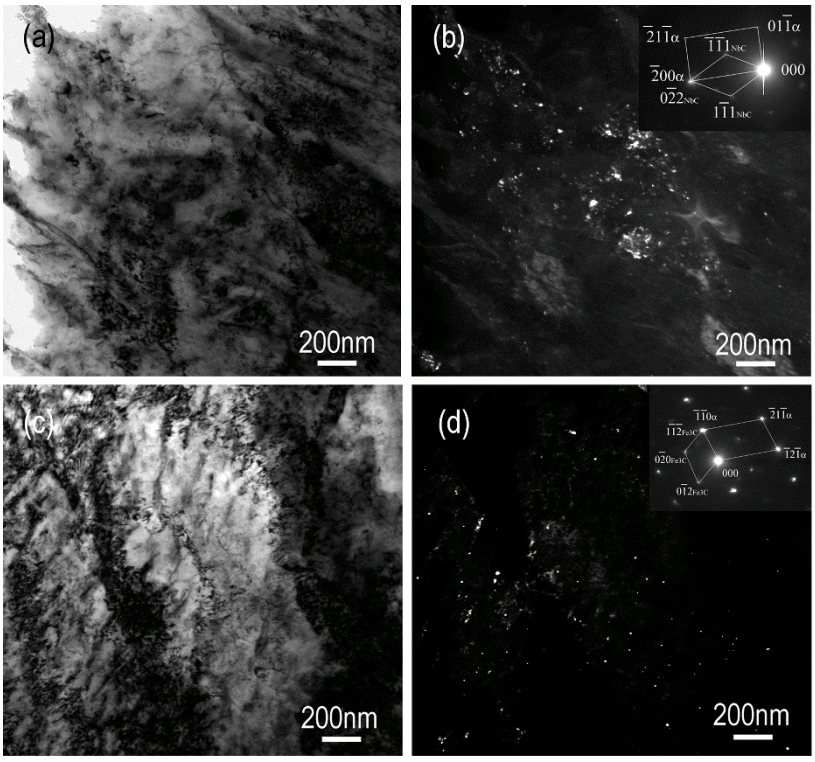

Figure 8. (**a**) and (**c**) BF images of carbides at 350 °C; (**b**) and (**d**) DF images of carbides, with the corresponding SAED pattern of NbC and Fe_3C inserted in (**b**) and (**d**), respectively.

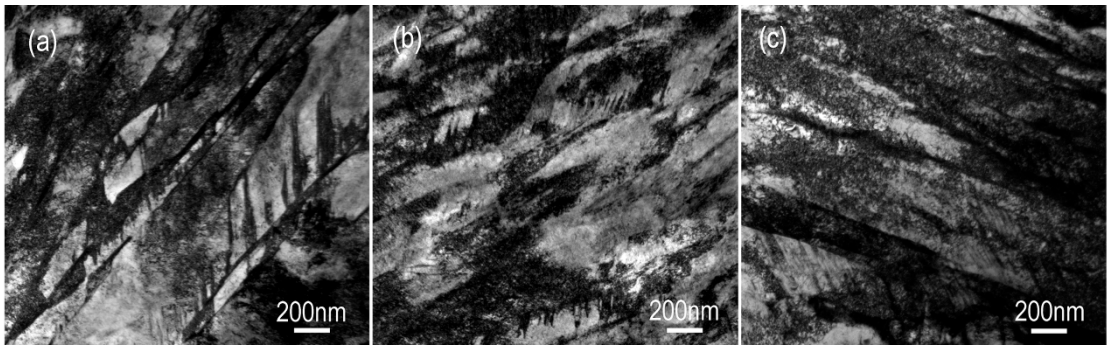

Figure 9. BF images of the deformed Q-P-T specimens at various temperatures: (**a**) 25 °C; (**b**) 200 °C and (**c**) 350 °C.

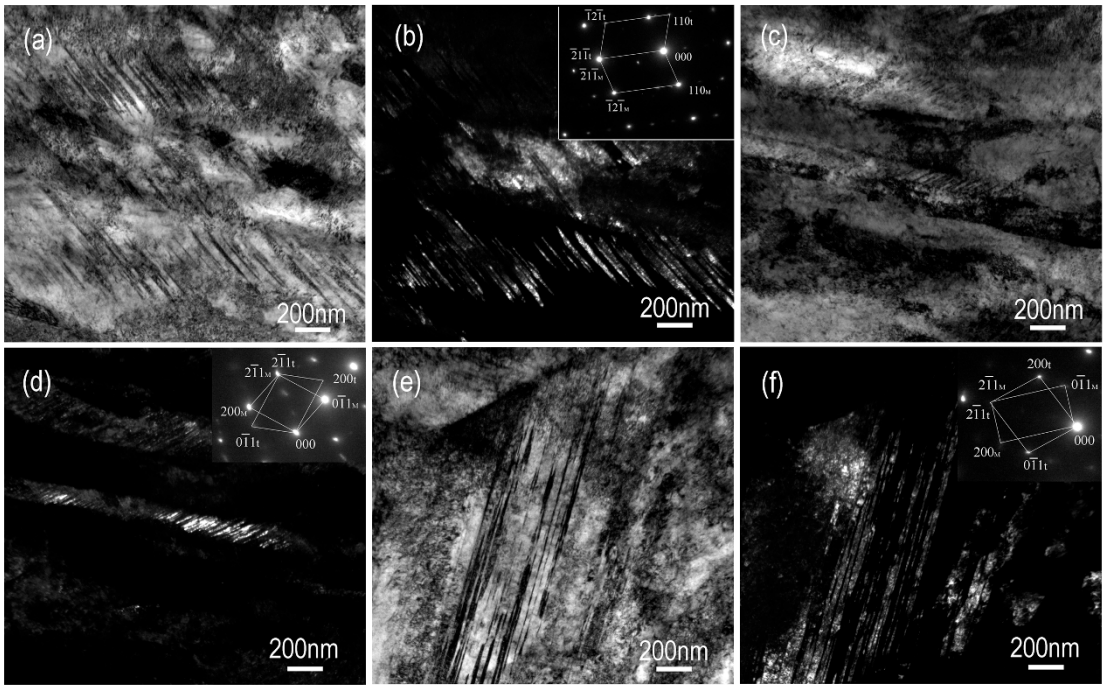

Figure 10. Transmission electron microscope (TEM) images of the deformed Q-P-T steels at various temperatures: (**a**) 25 °C, (**c**) 200 °C and (**e**) 350 °C, BF images; (**b**) 25 °C, (**d**) 200 °C and (**f**) 350 °C, DF images and the corresponding SAED pattern of twin-type martensite.

4. Conclusions

The relation, following high temperature deformation of a medium-carbon Q-P-T steel, between microstructures with their mechanical properties has been systematically studied through tensile tests, TEM and XRD. Here are our major conclusions.

1. The XRD and tensile test results clarified that the retained austenite showed excellent mechanical stability when it was deformed within the temperature range of 25–350 °C. The mechanical properties of the Q-P-T martensitic steel deformed at 350 °C were consistent with those at an ambient temperature. Consequently, The Q-P-T martensitic steel studied in this paper has a wider application prospect.

2. The maximum PSE (57,738 MPa%) of this Q-P-T steel occurred when the tensile samples were deformed at 200 °C. The TEM observation attributed a high ductility to the optimum combination of thermodynamic stability and the DARA and TRIP effects of the retained austenite at this temperature, whereas the high strength resulted from the precipitation of many NbC and ε carbides dispersed throughout the martensite matrix.

3. The UTS of this Q-P-T martensitic steel declined sharply at temperatures above 250 °C, because the V_{RA} of the retained austenite decreased gradually, and the retained austenite began to decompose. Moreover, the transitional ε carbides transformed into cementite. Si can effectively retard the formation of cementite at low temperatures, but it cannot prevent the precipitation of transitional carbides or the cementite formation at temperatures higher than 350 °C.

Author Contributions: K.Z. was responsible for designing, implementing the experiments, and writing this paper. M.Z., B.L. and P.L. provide characterization and testing support. W.L. and Y.R. participated in the data analysis and discussion. Moreover, I promise that all the authors have read and approved the final manuscript.

Funding: The work is financially supported by the National Key Research and Development Program of China (No. 2017YFB0306405).

Conflicts of Interest: The authors declare no conflict of interest.

References

1. Speer, J.G.; Matlock, D.K.; Cooman, B.C.; Schroth, J.G. Carbon Partitioning into Austenite after Martensite Transformation. *Acta Mater.* **2003**, *51*, 2611–2622. [CrossRef]
2. Speer, J.G.; Edmonds, D.V.; Rizzo, F.C.; Matlock, D.K. Partitioning of Carbon from Supersaturated Plates of Ferrite, with Application to Steel Processing and Fundamentals of the Bainite Transformation. *Solid State Mater. Sci.* **2004**, *8*, 219–237. [CrossRef]
3. Hsu, T.Y. Design of Structure, Composition and Heat Treatment Process for High Strength Steel. *Mater. Sci. Forum* **2007**, *2283*, 561–565.
4. Somani, M.; Porter, D.; Karjalainen, L.; Devesh, K. Evaluation of Dq & P Processing Route for the Development of Ultra-High Strength Tough Ductile Steels. *Int. J. Metall. Eng.* **2013**, *2*, 154–160.
5. Tan, X.D.; Xu, Y.B.; Yang, X.L.; Liu, Z.Q.; Wu, D. Effect of Partitioning Procedure on Microstructure and Mechanical Properties of a Hot-Rolled Directly Quenched and Partitioned Steel. *Mater. Sci. Eng. A* **2014**, *594*, 149–160. [CrossRef]
6. Yi, H.L.; Chen, P.; Hou, Z.Y.; Hong, N.; Cai, H.L.; Xu, Y.B.; Wu, D.; Wang, G.D. A Novel Design: Partitioning Achieved by Quenching and Tempering (Q–T & P) in an Aluminium-Added Low-Density Steel. *Scr. Mater.* **2013**, *68*, 370–374.
7. Wang, X.D.; Zhong, N.; Rong, Y.H.; Hsu, T.Y.; Wang, L. Novel Ultrahigh-Strength Nanolath Martensitic Steel by Quenching–Partitioning–Tempering Process. *J. Mater. Res.* **2009**, *24*, 260–267. [CrossRef]
8. Zhang, K.; Zhang, M.H.; Guo, Z.H.; Chen, N.L.; Rong, Y.H. A New Effect of Retained Austenite on Ductility Enhancement in High-Strength Quenching–Partitioning–Tempering Martensitic Steel. *Mater. Sci. Eng. A* **2011**, *528*, 8486–8491. [CrossRef]
9. Wang, Y.; Zhang, K.; Guo, Z.H.; Chen, N.L.; Rong, Y.H. A New Effect of Retained Austenite on Ductility Enhancement in High Strength Bainitic Steel. *Mater. Sci. Eng. A* **2012**, *552*, 288–294. [CrossRef]
10. Zhang, K.; Liu, P.; Li, W.; Ma, F.C.; Guo, Z.H.; Rong, Y.H. Enhancement of the Strength and Ductility of Martensitic Steels by Carbon. *Mater. Sci. Eng. A* **2018**, *716*, 87–91. [CrossRef]
11. Knijf, D.D.; Föjer, C.; Kestens, L.A.I.; Petrov, R. Factors Influencing the Austenite Stability During Tensile Testing of Quenching and Partitioning Steel Determined Via in-Situ Electron Backscatter Diffraction. *Mater. Sci. Eng. A* **2015**, *638*, 219–227. [CrossRef]
12. Moor, E.D.; Lacroix, S.; Clarke, A.J.; Penning, J.; Speer, J.G. Effect of Retained Austenite Stabilized Via Quench and Partitioning on the Strain Hardening of Martensitic Steels. *Metall. Mater. Trans. A* **2008**, *39*, 2586–2595. [CrossRef]
13. Wang, M.M.; Hell, J.C.; Tasan, C.C. Martensite Size Effects on Damage in Quenching and Partitioning Steels. *Scr. Mater.* **2017**, *138*, 1–5. [CrossRef]
14. Santofimia, M.J.; Zhao, L.; Petrov, R.; Kwakernaak, C.; Sloof, W.G.; Sietsma, J. Microstructural Development During the Quenching and Partitioning Process in a Newly Designed Low-Carbon Steel. *Acta Mater.* **2011**, *59*, 6059–6068. [CrossRef]
15. Zhong, N.; Wang, X.D.; Rong, Y.H.; Wang, L. Interface Migration between Martensite and Austenite during Quenching and Partitioning (Q&P) Process. *J. Mater. Sci. Technol.* **2006**, *22*, 751–754.

16. Masek, B.; Jirkova, H.; Hauserova, D.; Kucerova, L.; Klauberova, D. The Effect of Mn and Si on the Properties of Advanced High Strength Steels Processed by Quenching and Partitioning. *Mater. Sci. Forum* **2010**, *654*, 94–97. [CrossRef]
17. Cao, W.Q.; Wang, C.Y.; Shi, J.; Dong, H. Application of Quenching and Partitioning to Improve Ductility of Ultrahigh Strength Low Alloy Steel. *Mater. Sci. Forum* **2010**, *654*, 29–32. [CrossRef]
18. Schino, A.D.; Braccesi, C.; Cianetti, F.; Nunzio, P.D.; Mengaroni, S.; Rodriguez-Calvillo, P.; Cabrera, J.M. Manganese Effect on Q&P CMnSi Steels. *Mater. Sci. Forum* **2017**, *879*, 430–435.
19. Zhou, S.; Zhang, K.; Wang, Y.; Gu, J.F.; Rong, Y.H. The Mechanism of High Strength-Ductility Steel Produced by a Novel Quenching-Partitioning-Tempering Process and the Mechanical Stability of Retained Austenite at Elevated Temperatures. *Metall. Mater. Trans. A* **2012**, *43*, 1026–1034. [CrossRef]
20. Wang, Y.; Guo, Z.H.; Chen, N.L.; Rong, Y.H. Deformation Temperature Dependence of Mechanical Properties and Microstructures for a Novel Quenching–Partitioning–Tempering Steel. *J. Mater. Sci. Technol.* **2013**, *29*, 451–457. [CrossRef]
21. Wang, X.D.; Xu, W.Z.; Guo, Z.H.; Wang, L.; Rong, Y.H. Carbide Characterization in a Nb-Microalloyed Advanced Ultrahigh Strength Steel after Quenching–Partitioning–Tempering Process. *Mater. Sci. Eng. A* **2010**, *527*, 3373–3378. [CrossRef]
22. Koistinen, D.P.; Marburger, R.E. A General Equation Prescribing the Extent of the Austenite-Martensite Transformation in Pure Iron-Carbon Alloys and Plain Carbon Steels. *Acta Metall.* **1959**, *7*, 59–60. [CrossRef]
23. Sugimoto, K.I.; Kobayashi, M.; Hashimoto, S.I. Ductility and Strain-Induced Transformation in a High-Strength Transformation-Induced Plasticity-Aided Dual-Phase Steel. *Metall. Trans. A* **1992**, *23*, 3085–3091. [CrossRef]
24. Grässel, O.; Krüger, L.; Frommeyer, G.; Meyer, L.W. High Strength Fe–Mn–(Al, Si) Trip/Twip Steels Development—Properties—Application. *Int. J. Plasticity* **2000**, *16*, 1391–1409. [CrossRef]